Entrance Channel Effects in the Reaction of Aligned Ca(^1P) with HCl

Anthony J. H. M. Meijer,† Gerrit C. Groenenboom, and Ad van der Avoird*

Institute of Theoretical Chemistry, NSR Center, University of Nijmegen, Toernooiveld, 6525 ED Nijmegen, The Netherlands

Received: April 3, 1997; In Final Form: June 2, 1997[⊗]

In the (harpooning) reaction Ca(^1P) + HCl → CaCl($A^2\Pi$,$B^2\Sigma^+$) + H we study the effect of the long-range interactions between the multipole moments of HCl and the quadrupole moment of the Ca(^1P) atom, using semiclassical dynamics. The relative translational motion of the reagents is described by classical trajectories, while the rotation of HCl and the evolution of the Ca(^1P) state are treated quantum mechanically. We pay special attention to the influence of the alignment of the Ca(^1P) state, investigated experimentally by Rettner and Zare [*J. Chem. Phys.* **1982**, *77*, 2416]. We find orbital following when this excited state is polarized parallel (Σ) to the initial velocity vector, and we obtain adiabatic and nonadiabatic transitions into the Σ substate when the Ca(^1P) atom is initially polarized perpendicular (Π) to the beam. Simultaneously, there is a strong tendency of HCl to become orientationally localized, with H toward Ca. It is the anisotropy of the adiabatic potential energy surfaces and the polarization of the corresponding adiabatic states which relate these two phenomena. The initial polarization of the Ca(^1P) atom is clearly reflected in the orientational distribution of the HCl molecule when it reaches the harpooning radius. From a simple model for the chemical reaction we infer that these long-range effects have an important influence on the $A^2\Pi/B^2\Sigma^+$ branching ratio of the CaCl product, but we cannot quantitatively compute the (experimentally observed) effect of the Ca(^1P) alignment on this branching ratio.

I. Introduction

In this special issue on the stereodynamics of chemical reactions, it is shown in several contributions how a chemical reaction may be influenced by steering the orientation of the reagents. A beam of symmetric top (like) molecules can be oriented through the selection of a specific (*jkm*) state by means of a hexapole field.[1−6] The (partial) orientation or alignment of molecules can also be achieved by brute force methods.[7−9] Excited atoms have been prepared by electrical discharge[5,6,10,11] and by laser excitation;[12−15] in the latter case one can select specifically aligned substates by an appropriate choice of the laser polarization. The reaction Ca(^1P) + HCl → CaCl + H has been studied by Rettner and Zare[12,13] in a beam-gas setup with the polarized laser excitation method. The Ca(^1P) atoms were excited with Σ or Π polarization relative to their initial velocity vector, and the CaCl product emerged in its $A^2\Pi$ and $B^2\Sigma^+$ excited states which could be detected by looking at the luminescence. It was observed that the total luminescent cross section is insensitive to the Σ or Π polarization direction of the Ca(^1P) atoms but that the branching ratio of the CaCl($A^2\Pi$) and CaCl($B^2\Sigma^+$) exit channels depends markedly upon this direction. Parallel (Σ) polarization favors the formation of CaCl($B^2\Sigma^+$), while perpendicular (Π) polarization favors the CaCl($A^2\Pi$) exit channel. Additional information on the reaction of (^1D) excited Ca atoms with HCl has been obtained from crossed-beam experiments.[10,11] These studies addressed, in particular, the translational energy dependence of the reactive cross section and, in accompanying beam-gas measurements, the polarization of the CaCl($A^2\Pi$) and CaCl($B^2\Sigma^+$) products. The same reaction of Ca(^1P) and Ca(^1D) with HCl, leading to CaCl($A^2\Pi$,$B^2\Sigma^+$) + H, was also investigated by photoexcitation of the van der Waals complex Ca−HCl.[16,17,18] This is another way to control the (relative) orientation of the HCl molecule and the Σ or Π polarization of the excited Ca(^1P) and Ca(^1D) states. (Note that the degeneracy of the Σ and Π states is lifted in this complex.)

An essential question in the scattering studies of Ca + HCl (and other aligned systems) is, what happens to the initially prepared alignment of the reagents when they start interacting? Even before the onset of the actual chemical reaction, which in the case of Ca + HCl is probably initiated by a harpooning event,[11,13,19,20] there may be important long-range effects, such as orbital following[13,21−23] and reorientation.[5,24] In a series of quasi- and semiclassical calculations[25−28] on the reaction of (unaligned) Ca(^1D) with (*jkm*) state selected CH_3X (X = F, Cl, or Br), we have seen that such long-range effects—trapping, reorientation, and orbital following—are indeed occurring and have a marked influence upon the observed steric effect in the reactive cross section,[5,6,29] as well as on the energy dependence of this effect. Here, we present a similar semiclassical study of the reaction Ca(^1P) + HCl → CaCl($A^2\Pi$,$B^2\Sigma^+$) + H, and we look in particular at the effects of the initial Σ or Π polarization of the incoming Ca(^1P) atoms. This work is more or less complementary to the theoretical study in ref 11 on the reaction of Ca(^1D) atoms with HCl, which concentrates on the region where harpooning takes place and tries to explain the observed maximum in the reactive cross section as a function of energy. It was assumed in that study that the incoming HCl molecule is freely rotating, so that all its electric multipole moments are averaged out. In our work we investigate in particular what happens in the long range, before harpooning, and we consider the electrostatic interactions between the dipole, quadrupole, and octupole of HCl and the quadrupole moment of the Σ or Π prepared Ca(^1P) atom. On the basis of our Ca(^1D) + CH_3X work,[25−28] we expect that these electrostatic interactions will have important effects here, too.

† Current address: Department of Chemistry, Wayne State University, Detroit, MI, 48202.

* Corresponding author. In December 1996 at: Center for Interdisciplinary Research (ZiF), Universität Bielefeld, Germany.

⊗ Abstract published in *Advance ACS Abstracts,* September 15, 1997.

S1089-5639(97)01160-2 CCC: $14.00

II. Theory and Calculations

In the experiments by Rettner and Zare[12,13] on the reaction between Ca(^1P) and HCl, they excited the Ca atom into its ^1P state with polarized laser light, to obtain Σ or Π polarization relative to the initial velocity vector of the Ca beam. This polarization may change or the atom may become more or less unpolarized by the long-range interaction with HCl, and therefore, we include all three substates of the Ca(^1P) state in our calculations. We label these substates $|\mu\rangle$ with the magnetic quantum number μ relative to the laboratory or space-fixed (SF) frame with its z-axis along the initial velocity vector of the Ca atoms. Initially, $\mu = 0$ for the Σ polarized Ca(^1P) atoms and $\mu = \pm 1$ for the Π polarized atoms. We have also seen in our semiclassical studies on the reaction of Ca(^1D) with CH_3X that one of the effects of the long-range interactions between Ca and the dipolar molecule is trapping. This is the phenomenon that the atom approaching the molecule with a large impact parameter can be captured by the (partly attractive) potential, fly around it, and collide with it on the side or even at the back. If the Ca(^1P) would still have its original Σ or Π polarization, relative to the SF z-axis, this polarization would be seen differently by the approaching HCl molecule. Therefore, we also introduce a dimer frame (DF) with its z-axis pointing from the center of mass of HCl to the Ca atom, and we define the magnetic quantum number $\Lambda = 0, \pm 1$ of the Ca(^1P) state relative to the DF z-axis. For very large distance R of the reagents the DF frame coincides with the SF frame, of course. Since we want to investigate whether orbital following occurs, we monitor the populations of the Ca(^1P) substates labeled by μ as well as by Λ. And, since the asymptotically degenerate Ca(^1P) substates will be split by the electric field of HCl, we also obtain adiabatic states by diagonalization of the 3×3 interaction matrix (see below) for given geometries of the Ca−HCl complex.

Also, the rotation of the HCl molecule is treated quantum mechanically in our calculations. We start with HCl in $j = 0$, $j = 1$, or $j = 2$ with all values ($-j \le m \le j$) of m. Although the temperature in the experiment[12,13] is so high that the higher j states will be populated too, we expect to learn essentially what happens from the study of the evolution of these lower j states. We expect that the electric field of Ca(^1P) might be sufficiently strong to induce a "brute force" orientation of HCl. In our quantum mechanical description this becomes manifest by mixing of (j, m) states, possibly up to high values of j. We use a basis of spherical harmonics $|j, m\rangle = Y_m^{(j)}(\beta,\alpha)$, in which ($\beta$, α) are the polar angles of the HCl axis (pointing from H to Cl), and we include all functions with $j \le 38$. In our analysis of the results we monitor the populations of these HCl rotor states, with m defined either relative to the SF z-axis or relative to the DF z-axis. Moreover, we follow the orientational distribution of the HCl axis, with respect to both frames.

For the electrostatic interaction between Ca(^1P) and HCl we use the multipole expansion, in terms of spherical harmonics[30]

$$\hat{V}(\beta, \alpha, \boldsymbol{R}) = \sum_{l_a,l_b=0}^{\infty} \left[\frac{(2l_a + 2l_b + 1)!}{(2l_a)!\,(2l_b)!}\right]^{1/2} \times (-1)^{l_a} R^{-l_a-l_b-1} \sum_{m_a=-l_a}^{l_a} \sum_{m_b=-l_b}^{l_b} C^{(l_a+l_b)}_{-m_a-m_b}(\Theta, \Phi) \times \begin{pmatrix} l_a & l_b & l_a+l_b \\ m_a & m_b & -m_a-m_b \end{pmatrix} Q_0^{(l_a)} C_{m_a}^{(l_a)}(\beta,\alpha) \hat{Q}_{m_b}^{(l_b)} \quad (1)$$

Here, A labels the molecule and B the atom, $Q_0^{(l_a)}$ are the 2^{l_a}-pole moments of HCl, and $\hat{Q}_{m_b}^{(l_b)}$ are the multipole operators depending on the electronic coordinates $\boldsymbol{r}$ of the Ca atom. The functions $C_m^{(l)}$ are Racah normalized spherical harmonics. The polar angles (β, α) of the HCl axis and those (Θ, Φ) of the vector $\boldsymbol{R}$ that points from the HCl center of mass to the Ca nucleus are defined with respect to the SF frame. The quantity in large parentheses is a $3 - j$ symbol.[31] On the HCl molecule we include the dipole, quadrupole, and octupole moments with $l_a = 1$, 2, and 3, respectively. The only nonvanishing multipole moment of Ca(^1P) is the quadrupole, with $l_b = 2$. The elements of the 3×3 matrix for each of the five components ($m_b = -2$, -1, 0, 1, 2) of the operator $\hat{Q}_{m_b}^{(l_b)}$ with respect to the $\mu = -1$, 0, 1 substates are given by the Wigner−Eckart theorem[31]

$$\langle\mu|\hat{Q}_{m_b}^{(2)}|\mu'\rangle = (-1)^{1-\mu} \begin{pmatrix} 1 & 2 & 1 \\ -\mu & m_b & \mu' \end{pmatrix} \langle 1||Q^{(2)}||1\rangle \quad (2)$$

in terms of a single quantity $\langle 1||Q^{(2)}||1\rangle$, the reduced quadrupole matrix element for the ^1P state of Ca. Hence, we obtain an electrostatic long-range potential in which the Ca(^1P) atom is represented by the 3×3 quadrupole matrix. In this first study of the effect of long-range interactions in Ca + HCl, we will not include higher order interactions, such as induction or dispersion forces, since we expect that the effects of the (first order) electrostatic interactions will be dominant.

In our semiclassical calculations the quantum mechanical description of the electronic substates of the Ca(^1P) atom and the rotation of HCl is combined with classical trajectories for the relative translational motion of the atom and the molecule, as represented by the coordinate $\boldsymbol{R}$. The wave function is expanded in the product basis $|\mu,j,m\rangle \equiv |\mu\rangle|j,m\rangle$ defined above

$$|\Psi^{(\kappa)}(\boldsymbol{r}, \beta, \alpha; t)\rangle = \sum_{\mu=-1}^{1} \sum_{j=0}^{j_{max}} \sum_{m=-j}^{j} c_{\mu jm}^{(\kappa)}(t)|\mu, j, m\rangle \times \exp(-i\epsilon_j t/\hbar) \quad (3)$$

where $\epsilon_j = Bj(j + 1)$ are the rotational energies of HCl (B is the rotational constant). The superscript $\kappa \equiv (\mu_i,j_i,m_i,b)$ denotes the initial state, with (j_i, m_i) being the initial rotational quantum numbers of the HCl molecule, μ_i the initial electronic substate of the Ca atom, and b the impact parameter. The time evolution of the wave function is given by the time-dependent Schrödinger equation. The classical equations of motion for $\boldsymbol{R}$ are the so-called classical path equations.[32] More details on this, total energy conserving, formalism are given in refs 27 and 32.

Although the basis functions in the quantum mechanical part of the calculation are defined with respect to the SF system of axes, we can easily transform them to the dimer frame (DF) with its z-axis along the vector $\boldsymbol{R}$ and analyze the evolution of the electronic wave function in terms of the Ca(^1P) substates $|\Lambda\rangle$ defined with respect to the latter. Similarly, the evolution of the $|j, m\rangle$ rotor states of HCl can be followed in a basis with m components relative to $\boldsymbol{R}$, and the HCl orientation can be described by angles (β_R, α_R) defined relative to the DF frame.

When the two particles approach to a certain distance R_h, the harpooning radius, reaction is assumed to occur through a harpooning mechanism.[11,13] In fact, in this reaction there are two harpooning radii, which are important for the present work. The first one ("the outer harpooning radius") corresponds to the abstraction of the 4p electron and leads to ground-state products. The other ("the inner harpooning radius") corresponds to the abstraction of the 4s electron and leads to the CaCl($B^2\Sigma^+$/$A^2\Pi$) products studied. Since little is known about the dynamics in the reactive region, we use a very simple model to describe the influence of the Σ/Π preparation of the Ca(^1P) state and of the ensuing long-range effects on the final reactive cross sections

TABLE 1: Permanent Multipole Moments of the HCl Molecule in Atomic Units

l_a	$Q_0^{(l_a)}$	literature
1	−0.4351	−0.434,[a] −0.424,[b] −0.4301[d]
2	2.7448	2.732,[a] 2.72,[c] 2.78 ± 0.09[e]
3	−4.1174	−3.886,[a] −3.92[c]

[a] Calculated by an analytical MP2 formalism.[44] [b] Calculated by finite field MP4 with the inclusion of single, double, and quadruple excitations.[45] [c] Calculated[46] as in ref 45. [d] Experimental value.[47] [e] Experimental value.[48]

and on the $A^2\Pi/B^2\Sigma^+$ branching ratio. We analyze the orientational distribution of HCl and the Σ/Π content of the Ca(^1P) state—with respect to the DF system of axes—at the moment that R reaches the value R_h. The model neglects the possible effect of the harpooning at the outer radius on the Σ/Π population. From the distribution of the angle β_R relative to the vector $\boldsymbol{R}$ we can compute the reaction probability through the angle-dependent line of centers (ADLC) model.[33−36] Actually, since one expects no activation barrier for a reaction of this type, we use a version of the ADLC model with zero energy barrier, in which it is simply assumed that reaction occurs if the angle β_R at the moment of impact ($R = R_h$) is smaller than a certain cutoff angle β_0.[26−28] This defines a cone of reaction, $\beta_R \leq \beta_0$.

A reactive trajectory (collision) with $\beta_R \leq \beta_0$ at $R = R_h$ can lead to either of the two products, CaCl($A^2\Pi$) or CaCl($B^2\Sigma^+$). These exit channels are labeled by the projection, Λ_f, of the electronic angular momentum on the CaCl axis: $B^2\Sigma^+ \rightarrow \Lambda_f = 0$ and $A^2\Pi \rightarrow |\Lambda_f| = 1$. In the experiments by Rettner and Zare[12,13] on Ca + HCl and Ca + Cl_2 and also in other experiments,[16−18,37,38] it was found that this projection Λ_f on the symmetry axis of the product is correlated with the initial electronic angular momentum μ_i of the Ca(^1P) or Ca(^1D) state. In our model for the chemical reaction we analyze the character of the Ca(^1P) state at the moment of impact ($R = R_h$) and assume that a $\Lambda = 0$ state (Σ) leads to the CaCl($B^2\Sigma^+$) product, while a $|\Lambda| = 1$ state (Π) yields the CaCl($A^2\Pi$) product. In other words, the product branching ratio is determined by the relative populations of the Σ and Π states of the Ca(^1P) atom at $R = R_h$. We hope that, at least, the effect of the change in polarization of the Ca(^1P) state—caused by the long-range interactions—on the $A^2\Pi/B^2\Sigma^+$ branching ratio is correctly reflected in this manner. Although this model is extremely simple, it was successful in rationalizing the observed energy dependence of the steric effect in the reactions of Ca(^1D) with CH_3X,[5,6,29] as a consequence of the same type of long-range effects considered here.[25−28]

In order to obtain the reactive cross section for the two exit channels Λ_f ($A^2\Pi$ and $B^2\Sigma^+$), the trajectory calculations must be performed for a number of impact parameters b and for different initial rotational states (j_i, m_i). For a Σ polarized Ca(^1P) substate we start with $\mu_i = 0$ and for a Π polarized substate with $\mu_i = \pm 1$. For the cross sections with unpolarized Ca(^1P) atoms we must average over all values of μ_i.

III. Computational Details

We calculated the multipole moments of HCl up to the octupole at the level of second-order Møller−Plesset perturbation theory (MP2). The (experimental) bond length of HCl (1.2746 Å) was taken from ref 39. The basis for Cl was the same as in ref 28, and the H basis was the same as in ref 26. From the results listed in Table 1 it is clear that the calculated multipole moments are in good agreement with other calculations and with the experimental values. No experimental value for the octupole moment was available.

For the computation of the electronic wave functions and the quadrupole moment of the Ca atom in its ^1P excited state, we used the same multiconfiguration self-consistent-field (MCSCF) approach as in ref 26, including symmetry averaging over the 3-fold degenerate substates. We also used the same 117-orbital (15*s*,13*p*,13*d*,2*f*)/[11*s*,9*p*,13*d*,2*f*] basis as in our calculations on Ca(^1D).[26] This basis was optimized for Ca(^1D) at the restricted open-shell Hartree−Fock level. However, it also had to describe the $4p^2$ ^1D perturber state adequately, which contributes about 15%.[40] Therefore, we believe that we can use the same basis here to describe the 4*s*4*p* ^1P state. Moreover, this basis will also be suitable for the 3*d*4*p* ^1P perturber state, which contributes 15.5% to the 4*s*4*p* ^1P state.[40] We computed the expectation value of the $m_b = 0$ component of the quadrupole operator over the $\mu = 0$ component of the wave function by means of the linear response method, and from this quantity we obtained the reduced quadrupole matrix element by eq 2.

For the most extensive MCSCF calculation we performed—135 578 configuration state functions and 337 orbital rotations—the $^1P-^1S$ excitation energy was 23 979 cm^{-1}. This agrees very well with the experimental value of 23 652 cm^{-1}.[41] The ^1P quadrupole moment from this calculation was −10.060 au, which yields the reduced matrix element $\langle 1||Q^{(2)}||1\rangle = 27.55$ au. To our knowledge, no experimental results are available to compare with. Note that this value of the reduced quadrupole matrix element is considerably larger than the corresponding value ($\langle 2||Q^{(2)}||2\rangle = 15.77$ au) for the Ca(^1D) state computed in ref 26. Hence, the ^1P state is more diffuse, which might be expected because it corresponds to a basic electron configuration 4*s*4*p*, while the ^1D state corresponds to 3*d*4*s*.

In the beam-gas experiments by Rettner and Zare[12,13] the Ca atoms emerge, in an effusive beam, from an oven at a temperature of 1075 K, and they collide with (room temperature) HCl gas molecules. To obtain a representative scattering energy E, we take the most probable speed v of the Ca atoms at $T =$ 1075 K, and we assume that the HCl molecules have (average) speed zero. With this most probable speed v corresponds a kinetic energy $(1/2)m_{Ca}v^2 = kT$ [42] ($m_{Ca} = 40.080$ amu is the mass of Ca and k is the Boltzmann constant). The resulting scattering energy equals $E = (1/2)\mu v^2 = (\mu/m_{Ca})kT = 0.0438$ eV, where $\mu = m_{Ca}m_{HCl}/(m_{Ca} + m_{HCl})$ is the reduced mass of Ca + HCl, $m_H = 1.007\,825$ amu, and $m_{Cl} = 34.968\,85$ amu. Our choice of the translational energy is necessarily somewhat arbitrary, because the energy distribution in an effusive beam-gas experiment is very broad. Applying the formulas of Dagdigian *et al.*,[43] which take into account the velocity distributions of both the beam and the gas, we find that the average energy is actually about twice the above value, whereas the most probable energy is two-thirds of the above value.

For each electronic substate μ_i of the Ca(^1P) atom and for each (j_i, m_i) state of HCl, calculations were performed with 18 different impact parameters. These were equally distributed in b^2 with b between 0 and 14.43 bohrs. For impact parameters larger than 14.43 bohrs we found no reactive trajectories. Each trajectory started at $R = 30$ bohrs and was propagated up to the "inner" harpooning radius R_h (or to the point of closest approach). We assume here that $R_h = 6$ bohrs, which is in the range of values given in refs 11 and 13. Three cutoff angles, $\beta_0 = 120°$, 150°, and 180°, were chosen to determine the influence of the cone of reaction on the reactive cross sections and on the product branching ratio. The semiclassical calculations were performed with the same program as in ref 27. For details regarding numerical integration over the angles, the propagation, etc., see ref 27.

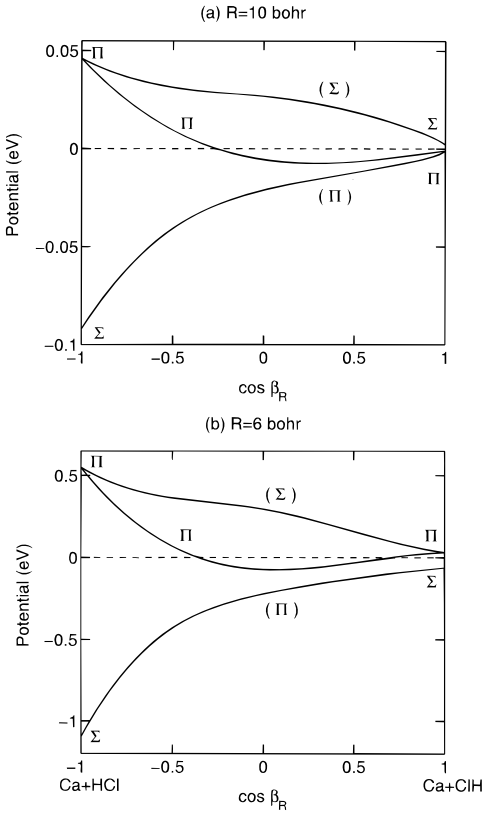

Figure 1. Cut through the adiabatic potential energy surfaces at R = 10.0 and 6.0 bohrs. The indicated (Σ/Π) character refers to the corresponding adiabatic eigenstates.

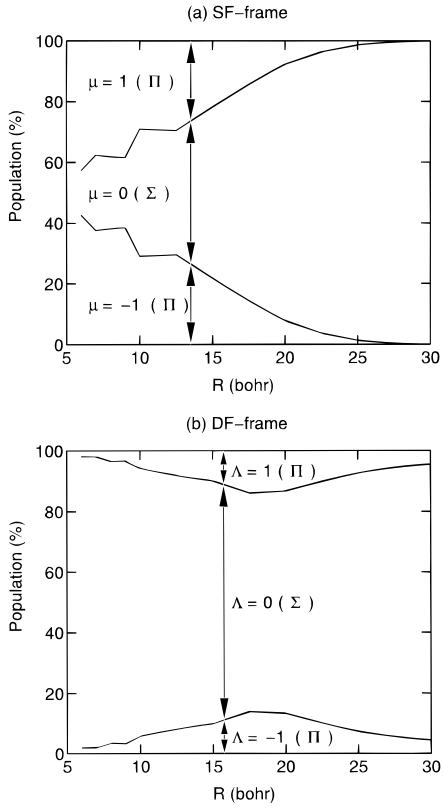

Figure 2. Evolution of the Ca(^1P) wave function along the trajectory with impact parameter b = 9 bohrs, starting with Σ polarized Ca (μ_i = 0) and the HCl molecule in (j_i, m_i) = (0, 0) at R = 30 bohrs. Panel *a* shows the populations of the components $|\mu\rangle$ with respect to the SF frame, and panel *b* shows the populations of the components $|\Lambda\rangle$ with respect to the DF frame.

IV. Results and Discussion

A. Adiabatic Interaction Potentials. Before we discuss the effects of the long-range interactions on the evolution of the electronic state of Ca and on the orientation of HCl, it is useful to look at some features of the long-range interaction potential of the Ca(^1P) + HCl system. As explained above, we computed the 3 × 3 matrix of the interaction operator in eq 1 over the three substates of Ca(^1P), with the multipole moments of the HCl molecule from Table 1 and the matrix elements of the Ca quadrupole operator given by the Wigner−Eckart theorem, eq 2. Diagonalization of this matrix yields three adiabatic potential energy surfaces, which are degenerate for $R \rightarrow \infty$. Cuts through these surfaces at R = 10 bohrs and R = 6 bohrs are shown in Figure 1. The labels Σ and Π on the three curves in each figure denote the symmetry character of the corresponding adiabatic eigenstates relative to $\boldsymbol{R}$. For the linear geometries with $\beta_R = 0$ and $\beta_R = \pi$ the eigenstates are pure Σ and Π states, with the latter being 2-fold degenerate. For other geometries the Σ/Π character is only approximate, except for the middle curve which remains purely Π_y for all angles. This (real) Π_y state cannot mix with the others, because it is the only antisymmetric one with respect to the plane of the Ca + HCl complex (the *xz*-plane).

For $\beta_R = \pi$, i.e., for the linear complex Ca−HCl, the attraction and repulsion are much stronger than for $\beta_R = 0$, i.e., for the Ca−ClH complex. This is caused by the opposite signs of the dipole, quadrupole, and octupole of HCl, which are, of course, related to the center-of-mass position and to the fact that the molecular *z*-axis was chosen to point from H to Cl. As a result, all these multipoles cooperate in their interaction with the Ca(^1P) state for the linear complex Ca−HCl and counteract each other for the linear Ca−ClH geometry. An illustration of this is that for $\beta_R = \pi$ the Σ state is lower than the Π state, independent of the distance R, while for $\beta_R = 0$ the order of these states is reversed between R = 10 bohrs and R = 6 bohrs. Obviously, it is the field of the HCl dipole that dominates at R = 10 bohrs, whereas the field of the quadrupole becomes more important at R = 6 bohrs. Equivalently, one may say that for given R the positive H atom is much closer to Ca in the Ca−HCl geometry than is the Cl atom in the Ca−ClH geometry and, therefore, that the interaction is much stronger in the former case. Hence, on the lowest potential surface there is a strong tendency to orient HCl with H toward the Ca atom ($\beta_R = \pi$), because this gives maximum energy lowering.

B. Evolution of the Ca(^1P) State. We will consider the evolution of the electronically excited Ca state with respect to both frames, SF and DF. Since these frames are nearly parallel for small impact parameters b, it is most instructive to look at trajectories with larger impact parameters. In Figures 2 and 3 we plotted the evolution of the Ca(^1P) state for a trajectory with b = 9 bohrs and the HCl molecule initiating in the rotational state with (j_i, m_i) = (0,0). Not every time step along the trajectory from 30 to 6 bohrs was analyzed; the populations of the μ and Λ substates were evaluated at intervals of 2.5 bohrs in the outer region and 1 bohr in the inner region. In Figure 2 the Ca atom is P_Σ prepared (μ_i = 0 at R = 30 bohrs), but one observes in the upper picture that already at $R \approx$ 14 bohrs about half of the population has gone into the P_Π substates with $\mu = \pm 1$. However, if we follow the evolution of the originally P_Σ substate with respect to the DF frame, i.e., the population of the substates labeled with Λ, we observe that the P_Σ (Λ = 0) substate remains almost fully intact. This is a clear-cut case of orbital following.

In Figure 3 the Ca atom is initially P_Π polarized ($\mu_i = \pm 1$). From the upper (SF) picture it seems that this P_Π substate first evolves into a nearly equal mixture of P_Π and P_Σ and then back

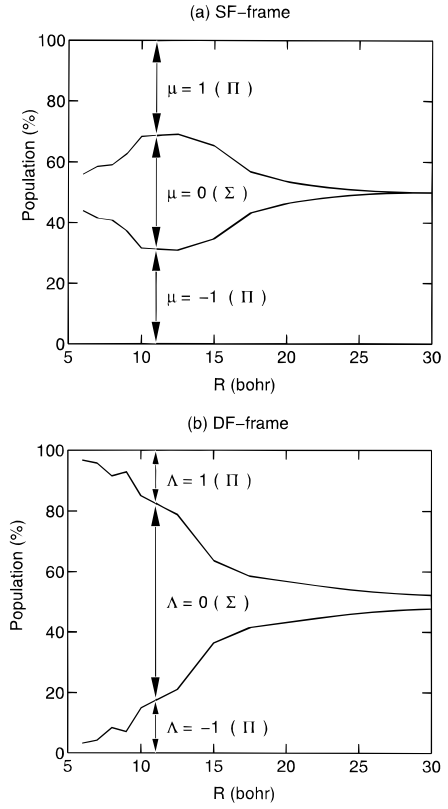

Figure 3. Evolution of the Ca(^1P) wave function as in Figure 2, but now starting from Π polarized Ca ($\mu_i = \pm 1$). Panel *a*: components $|\mu\rangle$ with respect to the SF frame. Panel *b*: components $|\Lambda\rangle$ with respect to the DF frame.

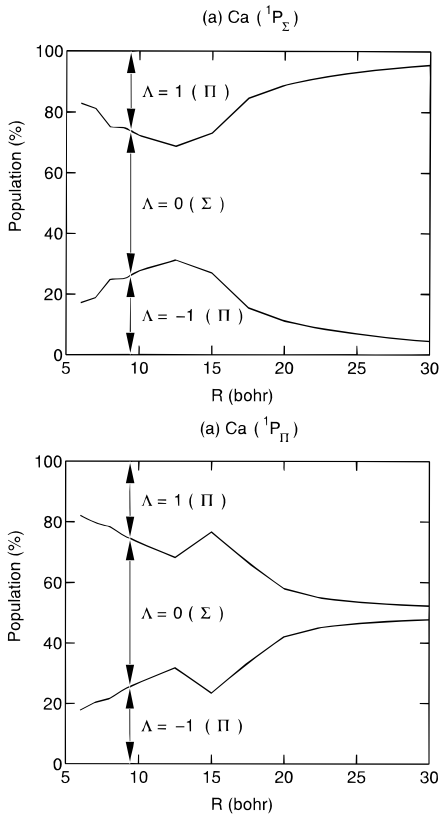

Figure 4. Evolution of the Ca(^1P) wave function as in Figure 2, but now starting with the HCl molecule in (j_i, m_i) = (1, 0) and Σ polarized Ca ($\mu_i = 0$) [panel *a*] or Π polarized Ca ($\mu_i = \pm 1$) [panel *b*]. Both panels show the components $|\Lambda\rangle$ with respect to the DF frame.

into P_Π. The lower (DF) picture is physically more clear, however: the P_Π substate becomes nearly pure P_Σ at smaller R. This could be caused by the strongly attractive Σ potential given by the lower curve in Figure 1, for $\beta_R \approx \pi$. Whether the HCl axis indeed orients itself in this direction with $\beta_R \approx \pi$ and whether the P_Π substate may undergo an adiabatic or nonadiabatic transition to the P_Σ state will be discussed in section IVC. In Figure 4a,b one can observe that the same trends—P_Σ remaining P_Σ, and P_Π evolving into P_Σ (always with respect to the DF frame)—occur also for HCl initially in (j_i,m_i) = (1, 0). The influence of the rotation of HCl is, however, that the strength of the effects is somewhat damped, possibly because the HCl axis cannot orient itself so easily as when it has zero angular momentum to begin with.

C. Orientation of HCl. In Figure 5 one can observe what happens to the (j_i,m_i) = (0, 0) state of HCl, when Ca is initially in P_Σ (in the upper picture) or in P_Π (in the lower picture). The change of the populations of all (j,m) states along the trajectory was plotted with m defined in the SF frame. In a similar plot (not shown) of the populations with m defined relative to the DF z-axis (the vector $\boldsymbol{R}$), it is obvious that the latter m value is better conserved, i.e., that the $m = 0$ substates stay relatively more populated. The total populations for each j are the same as in Figure 5, of course.

It is clear that states with $j > 0$ mix in already at very large R and that at smaller R even states with very high j are populated. The influence of the original P_Σ or P_Π polarization of Ca is most remarkable, however: for P_Σ prepared Ca atoms the populations of the $j > 0$ states grow much earlier (at larger R) than for P_Π preparation. The same remarkable difference between P_Σ and P_Π prepared Ca is seen in Figure 6. Mixing of the chosen rotor state of HCl, (j_i,m_i) = (1, 0) in this case, with other (j, m) states occurs for larger R when Ca is initially P_Σ polarized than when it is P_Π polarized.

Figures 7 and 8 display the corresponding angular distributions of the HCl axis, at $R = 10$, 8, and 6 bohrs. We plotted these distributions in the polar angles (β, α) relative to the SF frame, so that one can see in the pictures how well they follow the relative position of the Ca atom in the trajectory (marked by the arrow). In the plots we used the coordinates ($\pi - \beta$, $\pi + \alpha$), because we found that the HCl axis becomes preferentially oriented with H toward Ca ($\beta_R \approx \pi$), and this is more clearly visible with the coordinates of the inverted HCl axis (the ClH axis). In Figure 7 we start from (j_i,m_i) = (0, 0), i.e., a completely flat distribution, and in Figure 8 from (j_i,m_i) = (1, 0), i.e., a distribution proportional to $\cos^2 \beta$ and flat in α. Even the latter initial distribution is much flatter than the distributions shown in Figures 7 and 8, however.

Two effects strike the eye in Figure 7. First, there is strong orientational localization of HCl with H toward Ca. The cause of this "brute force" orientation of the HCl axis is the strongly attractive lower adiabatic potential in Figure 1, which corresponds to a P_Σ electronic state on Ca near $\beta_R = \pi$. This potential is much stronger than any external potential used to obtain "brute force" orientation of polar molecules.[7−9] So, obviously, the Ca(^1P) atom becomes (re)prepared by the electrostatic interactions with HCl. It stays in the P_Σ state—by orbital following—if it was prepared in P_Σ and undergoes a transition to the P_Σ state if it was originally in P_Π. This transition may be a nonadiabatic transition from the two higher adiabatic surfaces to the lowest surface, but it can also be an adiabatic process, because there is Σ−Π mixing in the lowest adiabatic state; *cf.* Figure 1. This is in contrast with the case of a neutral or ionic ^1S atom interacting with another atom in a P state,[22,23] where Σ and Π are the exact symmetries of the adiabatic potential curves. So, in that case, orbital following must occur, unless there is a nonadiabatic transition when the Σ−Π splitting becomes of the

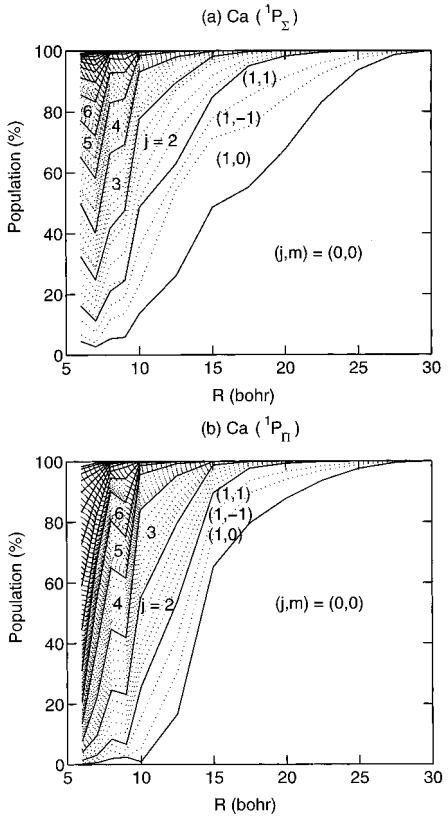

Figure 5. Evolution of the populations of the (j,m) rotor states of HCl along the trajectory with impact parameter $b = 9$ bohrs, starting with the HCl molecule in (j_i, m_i) = (0, 0) at $R = 30$ bohrs and Σ polarized Ca(^1P) ($\mu_i = 0$) [panel *a*] or Π polarized Ca(^1P) ($\mu_i = \pm 1$) [panel *b*]. The areas between the closed curves are the populations for each j, summed over m; the areas between the dotted lines refer to the individual m substates, defined with respect to the SF frame.

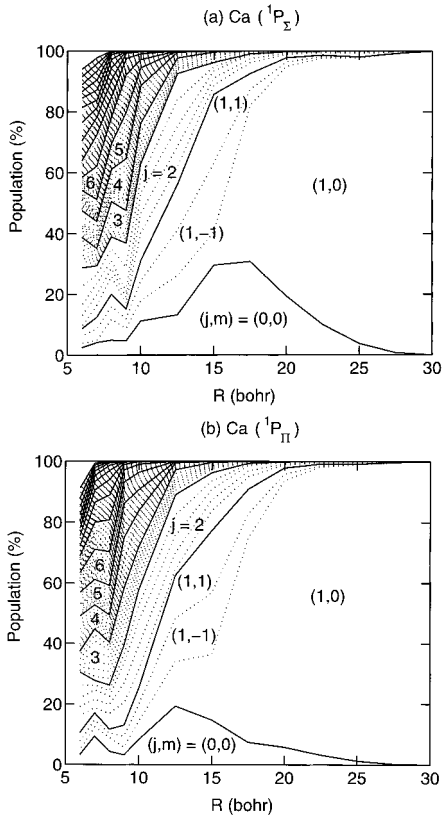

Figure 6. Evolution of the populations of the (j, m) rotor states of HCl as in Figure 5, but now starting with the HCl molecule in (j_i, m_i) = (1, 0) and Σ polarized Ca ($\mu_i = 0$) [panel *a*] or Π polarized Ca ($\mu_i = \pm 1$) [panel *b*].

same size as the Coriolis coupling terms. The (re)preparation of the Ca(^1P) state and the orientation of the HCl axis are coupled processes: the electrostatic potential of HCl will be so strong only when HCl is no longer freely rotating, and it is most attractive when the Ca(^1P) state has Σ symmetry and $\beta_R \approx \pi$. This leads to the formation of a nearly linear Ca−HCl "complex".

The second phenomenon that clearly emerges from Figure 7 is that, in spite of the orbital repreparation effects, it makes a large difference whether the original polarization of Ca(^1P) is Σ or Π. The orientational localization of HCl is stronger and occurs earlier for the initial P_Σ state than for the P_Π state. We already noticed this effect in the mixing of the (j, m) states in Figures 5 and 6. We believe that the (adiabatic or nonadiabatic) repreparation of the P_Π state into P_Σ occurs only slowly during the propagation of the trajectory, because it takes some time for the HCl molecule to become oriented and produce the strong electric field that lowers the energy of the Σ state. By consequence, the Ca P_Π state interacting with HCl will have a longer memory of its original polarization; the typical time lag is the time of rotation of HCl. From the rotational constant of HCl ($B = 10.59$ cm^{-1} = 317.5 GHz) it follows that this time of rotation is typically about 3 ps, while the propagation time from $R = 30$ bohrs to $R = 6$ bohrs in our calculations is about 2 ps.

If we compare Figure 7 with the corresponding results for Ca(^1D) + CH_3F in Figures 8 and 9 of ref 27, we observe that also the symmetry axis of CH_3F becomes orientationally localized by the long-range interactions with the excited Ca atom but that the orientation of the CH_3F axis lags much more behind the position of the Ca atom than the orientation of the HCl axis in the present case. This is in line with the moments of inertia: HCl has a much larger rotational constant B, i.e., a considerably smaller moment of inertia, than CH_3F (of which the relevant rotational constant is $B = 0.85$ cm^{-1}). Moreover, the relative velocity of CH_3F and Ca in the experiments of refs 5, 6, and 29 is larger than the relative velocity of HCl and Ca in the present case, and we saw already in ref 27 that the change in the orientation of the CH_3F axis depends on this relative velocity.

In Figure 8 one can observe similar orientational localization of HCl for an initial state with (j_i,m_i) = (1, 0). The localization is somewhat less pronounced than in Figure 7 and the resulting angular distribution is somewhat more complex, due to the initial angular momentum of HCl. But there is also a marked dependence on the initial Σ or Π polarization of the Ca(^1P) atom, in the same direction as for (j_i,m_i) = (0, 0).

D. Reactive Cross Sections and Branching Ratios. In Table 2 we listed the reactive cross sections and the $A^2\Pi/B^2\Sigma^+$ branching ratios for cutoff angles β_0 of 120° and 150°. The total reactive cross sections were obtained by counting the trajectories that reach the harpooning radius $R_h = 6$ bohrs and analyzing the final angular distribution of HCl (transformed to the DF frame): reaction occurs if $\beta_R \leq \beta_0$. The branching ratio follows directly from the ratio between the final populations of the Σ and Π components of the Ca(^1P) state relative to $\boldsymbol{R}$; see section II. We cannot attribute any quantitative significance to the total reactive cross sections computed in this manner, not only because of the simple model used for the chemical reaction but also because we took only a single scattering energy—instead of representing the complete velocity distribution—and we did not average over all the initial j states of HCl which are thermally populated. The results given, for $j_i = 0$, $j_i = 1$, and $j_i = 2$, were averaged over the substates with $-j_i \leq m_i \leq j_i$.

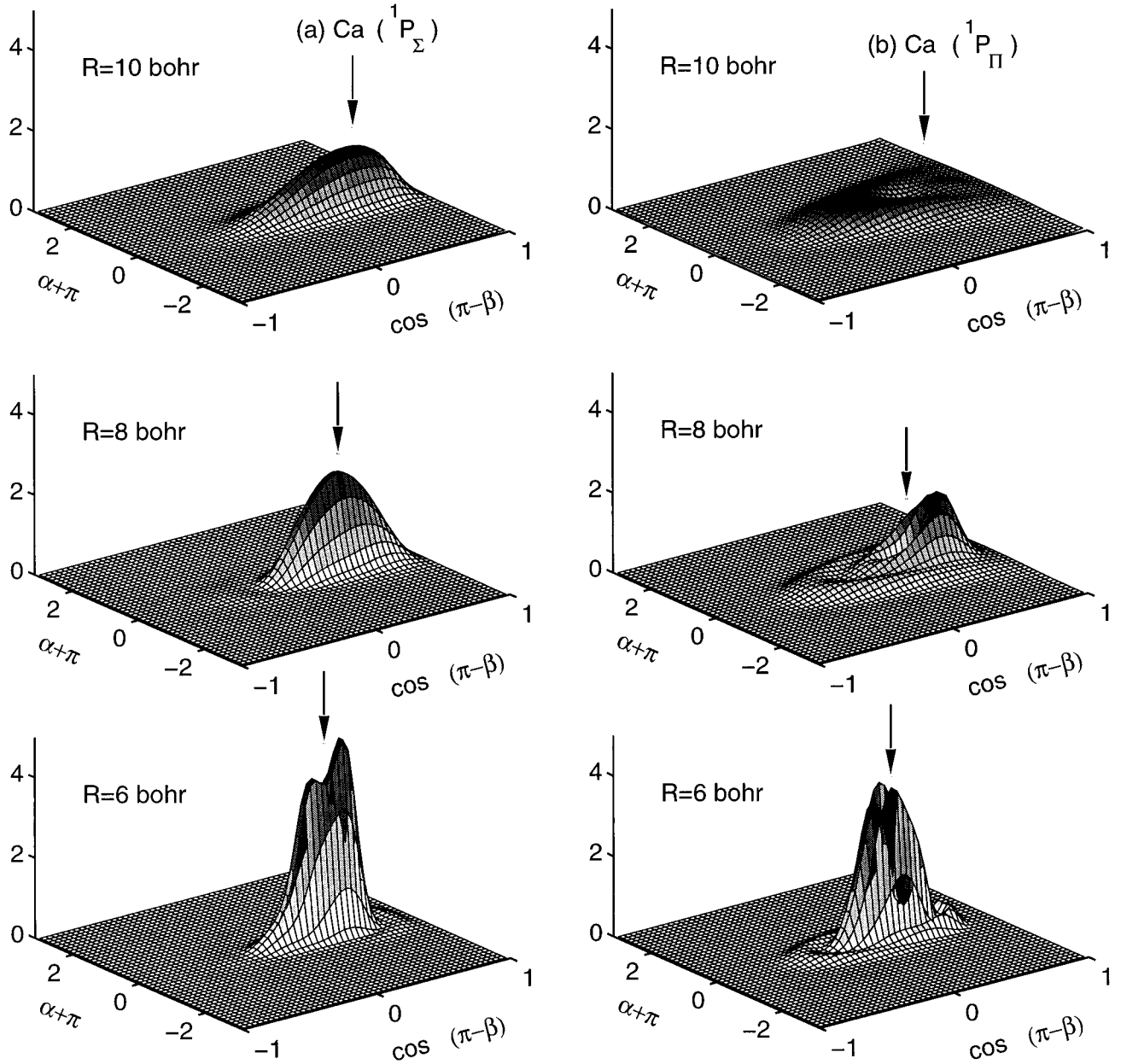

Figure 7. Evolution of the angular distribution of HCl along the trajectory with impact parameter $b = 9$ bohrs, starting with the HCl molecule in $(j_i, m_i) = (0, 0)$ and Σ polarized Ca(^1P) ($\mu_i = 0$) [panel *a*] or Π polarized Ca(^1P) ($\mu_i = \pm 1$) [panel *b*]. Distributions are given for $R = 10$, 8, and 6 bohrs, in terms of the polar angles (β, α) of the HCl axis with respect to the SF frame. The arrow indicates the position of the Ca atom.

The total reactive cross sections depend very strongly on the cutoff angle β_0. Many of the trajectories that arrive at $R = R_h$ have β_R values close to 180°, because of the orientational localization of HCl. As shown in section IVC, this occurs in particular for $j_i = 0$. For the reaction model with $\beta_0 = 180°$ all trajectories arriving at $R = R_h$ are reactive, of course, but already a narrowing of the cone-of-reaction to $\beta_0 = 150°$ leads to many trajectories becoming nonreactive. Since we cannot trust the total cross sections, we might try to infer the best value of β_0 from the $A^2\Pi/B^2\Sigma^+$ branching ratio, without alignment of the Ca(^1P), and then to use this value to study the influence of alignment. Experimentally,[12,13] the *A*/*B* ratio was observed to be 2.5 ± 0.1. From the average values in Table 2 one observes that this *A*/*B* ratio is obtained for β_0 between 120° and 150°. Taking into account that the experimental value is an average over all initial conditions (limited to $j_i = 0$, $j_i = 1$, and $j_i = 2$, in our case), it follows that β_0 close to 150° is probably the most realistic cutoff angle. For the reaction of Ca(^1D) with CH_3Cl we found the same value.[28]

Let us now ask the question: how are the reactive cross section and the *A*/*B* branching ratio affected by the Σ or Π polarization of the Ca(^1P) atom? In the experiment of Rettner and Zare[12,13] it was found that the total reactive cross section was hardly affected by the Ca(^1P) orbital polarization. In Table 2 we find changes of typically ±10% with respect to the average total cross sections, for $\beta_0 \approx 150°$. Although Rettner and Zare found a distinct influence of the Ca(^1P) polarization on the *A*/*B* branching ratio, we remind the reader that this effect was small: 100% Σ polarization gave just a few percent more of the $B^2\Sigma^+$ product, while 100% Π polarization gave a few percent more of the $A^2\Pi$ product. In Table 2 one can see that there are indeed marked effects of the initial Ca(^1P) polarization on the branching ratios, but also that these effects depend very sensitively on the cutoff angle β_0 and on the value of j_i. For instance, for $j_i = 0$ a cutoff angle of 120° gives an effect in the same direction as the experiment, whereas a cutoff angle of 150° gives an effect in the opposite direction. For $j_i > 0$, which seems more representative, with a cutoff angle of 150°, the effect

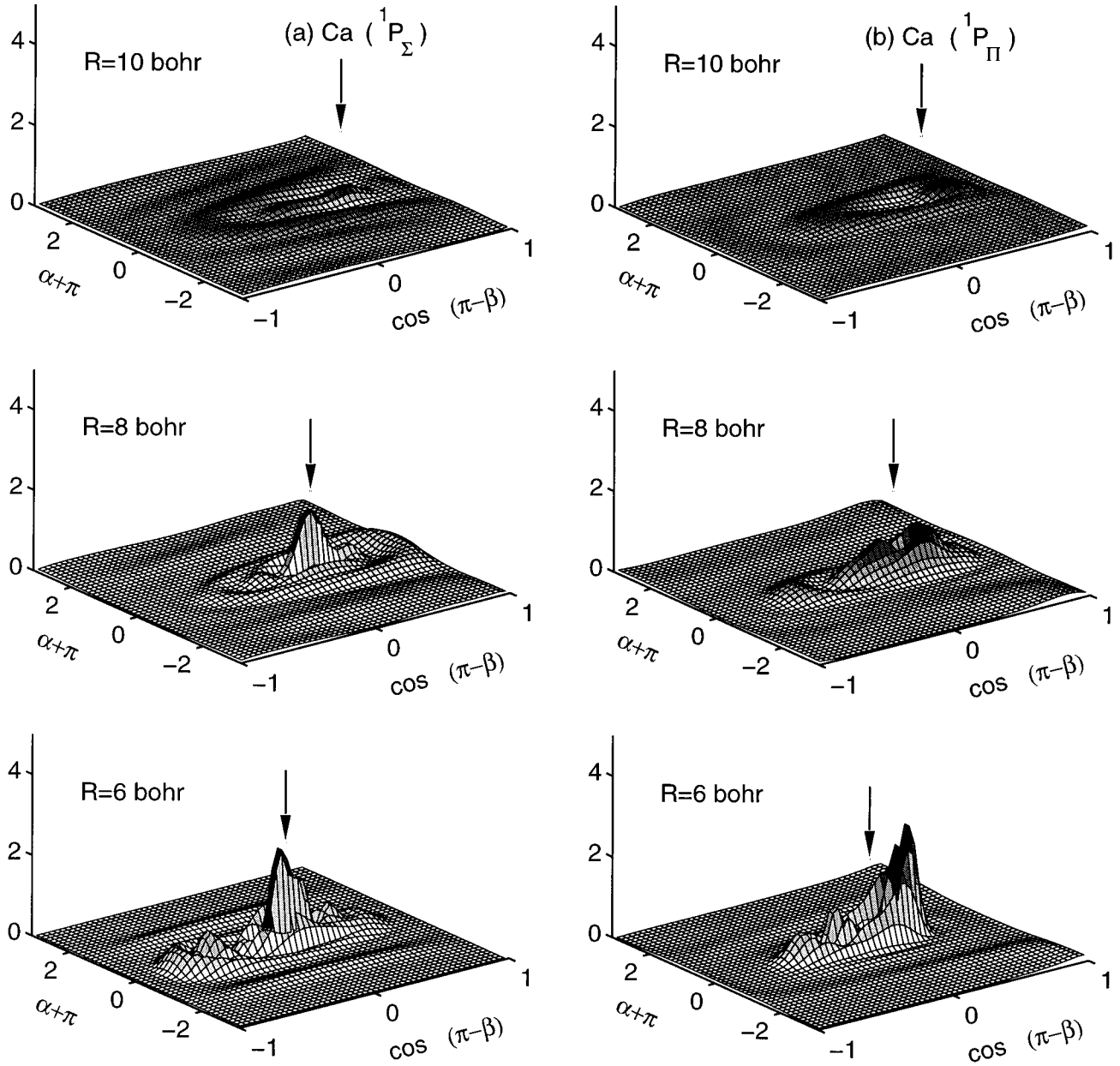

Figure 8. Evolution of the angular distribution of HCl as in Figure 7, but now starting with the HCl molecule in (j_i, m_i) = (1, 0) and Σ polarized Ca ($\mu_i = 0$) [panel *a*] or Π polarized Ca ($\mu_i = \pm 1$) [panels *b*].

TABLE 2: Reactive Cross Sections and $A^2\Pi/B^2\Sigma^+$ Branching Ratios for Cutoff Angles $\beta_0 = 150°$ (120°)

		HCl		
Ca(^1P)	CaCl	$j_i = 0$	$j_i = 1$	$j_i = 2$
P_Σ	total	59 (12)	226 (113)	249 (152)
	$A^2\Pi/B^2\Sigma^+$	1.0 (1.7)	1.6 (32)	2.2 (22)
P_Π	total	83 (7.7)	187 (124)	204 (107)
	$A^2\Pi/B^2\Sigma^+$	0.37 (15)	2.8 (61)	1.7 (20)
average	total	75 (9.1)	200 (120)	219 (122)
	$A^2\Pi/B^2\Sigma^+$	0.50 (4.0)	2.2 (48)	1.8 (21)

follows the experimental trend for $j_i = 1$ and the opposite trend for $j_i = 2$. Given this extreme sensitivity on the parameters of our crude model for the chemical reaction, we must conclude that this model is too simple to predict the effect of the Ca(^1P) polarization on the product branching ratio. Hence, we cannot draw any direct conclusions on the effect of the long-range interactions on this branching ratio on the basis of our calculations. We clearly find, however, that it is relevant for the product branching ratio *A*/*B* that the initial Ca(^1P) polarization is to a large extent destroyed and that the HCl axis has no longer a random angular distribution. Both these effects are due to the long-range interactions, and they occur before the actual start of the chemical reaction. But, at the same time, we observe that the effects of the initial Ca(^1P) polarization are still clearly visible in the angular distribution of HCl, when the reagents arrive at the harpooning radius. Moreover, the effect of the (mostly attractive) long-range interactions is that many more trajectories will arrive at this radius, because of "trapping".[25]

V. Conclusions

We studied entrance channel effects in the reaction Ca(^1P) + HCl → CaCl + H by means of semiclassical calculations. The relative translational motion of the reagents was described by classical trajectories, while, simultaneously, the evolution of the (asymptotically degenerate) electronic substates of the Ca(^1P) atom and of the rotations of HCl was determined by the time-dependent Schrödinger equation. We looked, in particular, at the effect of the electrostatic long-range interactions on the initially prepared Σ or Π polarization of the Ca(^1P) atom and

on the (originally random) orientation of the HCl axis. Such long-range interactions occur between the dipole and higher multipole moments of the HCl molecule and the quadrupole moment of the Ca(^1P) substates.

We found the following interesting effects:

1. If the Ca atom is excited to the ^1P state with Σ polarization relative to its initial velocity vector, it tends to keep this polarization, but rather with respect to the vector $\boldsymbol{R}$ between the HCl center of mass and the Ca atom. This is a clear-cut case of orbital following. If the Ca atom is ^1P excited with Π polarization, it tends to convert (both by adiabatic and nonadiabatic transitions) into a P_Σ state, again relative to the axis $\boldsymbol{R}$.

2. At the same time, the HCl axis undergoes a "brute force" orientational localization, with the H atom preferentially pointing toward Ca. This localization is strongest when we start with HCl in its $(j,m) = (0, 0)$ state.

These effects are related through the coupling between the Σ and Π character of the three adiabatic states of Ca(^1P) + HCl (which are degenerate for $R \rightarrow \infty$) and the dependence of the corresponding potential surfaces on the angle β_R between the HCl axis and the vector $\boldsymbol{R}$. The observed consequences of the long-range interactions are mainly determined by the fact that the lowest adiabatic surface is strongly attractive and has Σ character in the region of nearly linear Ca−HCl.

We also found that, in spite of these important (re)orientation effects, it makes a substantial difference in the resulting angular distribution of HCl whether the Ca(^1P) atom starts with Σ or with Π polarization. The effect of the Ca(P_Σ) atom on the orientation of the HCl axis starts earlier than the effect of the Ca(P_Π) atom, and the orientational distribution of HCl remains dependent on the initial polarization of Ca(^1P) down to the smallest distance considered (i.e., the harpooning radius, estimated at $R_h = 6$ bohrs). This "memory" effect is due to the time that it takes to (re)orient the HCl molecule.

Finally, we tried to relate the observed long-range effects to the experimentally measured[12,13] dependence of the CaCl($A^2\Pi$)/CaCl($B^2\Sigma^+$) product branching ratio on the initial Σ or Π polarization of the Ca(^1P) atom. Very little is known, however, about the chemical reaction process, and we had to use a strongly simplified model for this reaction. Although we found that the repolarization of the Ca(^1P) atom and the orientational localization of HCl induced by the long-range interactions and, in particular, the differential effects of the initial Σ or Π polarization of Ca, have an important influence on the A/B product branching ratio, our reaction model proved too simple to make quantitative predictions of the branching ratio.

Acknowledgment. A.J.H.M.M. thanks the Netherlands Foundation for Chemical Research (SON) and the Netherlands Organization for the Advancement of Research (NWO) for financial support. G.C.G. thanks the Royal Netherlands Academy for Arts and Sciences (KNAW), also for financial support.

References and Notes

(1) Kramer, K. H.; Bernstein, R. B. *J. Chem. Phys.* **1965**, *42*, 767.
(2) Brooks, P. R.; Jones, E. M. *J. Chem. Phys.* **1966**, *45*, 3449.
(3) Parker, D. H.; Chakravorty, K. K.; Bernstein, R. B. *J. Phys. Chem.* **1981**, *85*, 466.
(4) Stolte, S.; Chakravorty, K. K.; Bernstein, R. B.; Parker, D. H. *Chem. Phys.* **1982**, *71*, 353.
(5) Janssen, M. H. M.; Parker, D. H.; Stolte S. *J. Phys. Chem.* **1991**, *95*, 8142.
(6) Janssen, M. H. M.; Parker, D. H.; Stolte S. *J. Phys. Chem.* **1996**, *100*, 16066.
(7) Friedrich, R.; Herschbach, D. R. *Nature* **1991**, *353*, 412.
(8) Loesch, H. J.; Remscheid, A. *J. Chem. Phys.* **1990**, *93*, 4779.
(9) Loesch, H. J. *Annu. Rev. Phys. Chem.* **1995**, *46*, 555.
(10) Menéndez, M.; Garay, M.; Verdasco, E.; González Ureña, A. *J. Chem. Soc., Faraday Trans.* **1993**, *89*, 1493.
(11) de Castro Vítores, M.; Candori, R.; Pirani, F.; Aquilanti, V.; Menéndez, M.; Garay, M.; González Ureña, A. *J. Phys. Chem.* **1996**, *100*, 7997.
(12) Rettner, C. T.; Zare, R. N. *J. Chem. Phys.* **1981**, *75*, 3636.
(13) Rettner, C. T.; Zare, R. N. *J. Chem. Phys.* **1982**, *77*, 2416.
(14) Hale, M. O.; Leone, S. R. *J. Chem. Phys.* **1983**, *79*, 3352.
(15) Kovalenko, L. J.; Robinson, R. L.; Leone, S. R. *J. Chem. Soc., Faraday Trans. 2* **1989**, *85*, 939.
(16) Soep, B.; Whitham, C. J.; Keller, A.; Visticot, J. P. *J. Chem. Soc., Faraday Trans.* **1991**, *91*, 191.
(17) Soep, B.; Abbès, S.; Keller, A.; Visticot, J. P. *J. Chem. Phys.* **1992**, *96*, 440.
(18) Keller, A.; Lawruszczuk, R.; Soep, B.; Visticot, J. P. *J. Chem. Phys.* **1996**, *105*, 4556.
(19) Herschbach, D. R. *Adv. Chem. Phys.* **1966**, *10*, 319.
(20) Levine, R. D.; Bernstein, R. B. *Molecular Reaction Dynamics*; Oxford University Press: Oxford, 1987.
(21) Hertel, I. V. *Adv. Chem. Phys.* **1981**, *45*, 341.
(22) Grosser, J. *J. Phys. B: At. Mol. Phys.* **1981**, *14*, 1449.
(23) Schatz, G. C.; Kovalenko, L. J.; Leone, S. R. *J. Chem. Phys.* **1989**, *91*, 6961.
(24) Bernstein, R. B.; Levine, R. D. *J. Phys. Chem.* **1989**, *93*, 1687.
(25) Groenenboom, G. C.; Meijer, A. J. H. M. *J. Chem. Phys.* **1994**, *101*, 7592.
(26) Meijer, A. J. H. M.; Groenenboom, G. C.; Van der Avoird, A. *J. Chem. Phys.* **1994**, *101*, 7603.
(27) Meijer, A. J. H. M.; Groenenboom, G. C.; Van der Avoird, A. *J. Chem. Phys.* **1996**, *105*, 2247.
(28) Meijer, A. J. H. M.; Groenenboom, G. C.; Van der Avoird, A. *J. Phys. Chem.* **1996**, *100*, 16072.
(29) Janssen, M. H. M. Ph.D. Thesis, KUN Nijmegen NL, 1989.
(30) Van der Avoird, A.; Wormer P. E. S.; Mulder, F.; Berns, R. M. *Top. Curr. Chem.* **1980**, *93*, 1.
(31) Edmonds, A. R. *Angular Momentum in Quantum Mechanics*; Princeton University Press: Princeton, 1957.
(32) Billing, G. D. *Int. Rev. Phys. Chem.* **1994**, *13*, 309.
(33) Levine, R. D.; Bernstein, R. B. *Chem. Phys. Lett.* **1984**, *105*, 467.
(34) Smith, I. W. M. *J. Chem. Educ.* **1982**, *59*, 9.
(35) Pollak, E.; Wyatt, R. E. *J. Chem. Phys.* **1983**, *78*, 4464.
(36) Janssen, M. H. M.; Stolte, S. *J. Phys. Chem.* **1987**, *91*, 5480.
(37) Menzinger M. In *Selectivity in Chemical Reactions*; Whitehead, J. C., Ed.; NATO ASI Series C; Kluwer Academic: Dordrecht, 1988; Vol. I, p 457.
(38) Menzinger, M. *Pol. Phys. Acta* **1988**, *A73*, 85.
(39) Herzberg, G. *Molecular Spectra and Molecular Structure*; Krieger: Malabar, 1991; Vol. I.
(40) Vaeck, N.; Godefroid, M.; Hansen, J. E. *J. Phys. B: At., Mol. Opt. Phys.* **1991**, *24*, 361.
(41) Moore, C. E. *NBS Reference Data Series*; US Government Printing Office: Washington, DC, 1949; No. 35, Vol. I.
(42) Atkins, P. W. *Physical Chemistry*, 3rd ed.; Oxford University Press: Oxford, 1986; p 650.
(43) Dagdigian, P. J.; Cruse, H. W.; Zare, R. N. *J. Chem. Phys.* **1975**, *62*, 1824.
(44) Hettema, H.; Wormer, P. E. S.; Thakkar, A. J. *Mol. Phys.* **1993**, *80*, 533.
(45) Maroulis, G. *Mol. Phys.* **1991**, *74*, 131.
(46) Maroulis, G. *J. Phys. B* **1991**, *24*, L117.
(47) Kaiser, E. W. *J. Chem. Phys.* **1970**, *53*, 1686.
(48) de Leeuw, F. H.; Dymanus, A. *J. Mol. Spectrosc.* **1973**, *48*, 427.